Fourier-transform spectroscopy, direct-potential-fit, and electronic structure calculations on the entirely perturbed $(4)^1\Pi$ state of RbCs

I. Klincare, A. Kruzins, M. Tamanis, and R. Ferber*
Laser Center, Department of Physics, University of Latvia, 19 Rainis blvd, Riga LV-1586, Latvia

E. A. Pazyuk and A. V. Stolyarov†
Department of Chemistry, Moscow State University, 119991, GSP-2, Moscow, Leninskie gory 1/3, Russia

(Dated: October 1, 2018)

We performed a high-resolution Fourier-transform spectroscopic study of the $(4)^1\Pi$ state of the RbCs molecule by applying two-step $(4)^1\Pi \leftarrow A^1\Sigma^+ \sim b^3\Pi \leftarrow X^1\Sigma^+$ optical excitation followed by observation of the $(4)^1\Pi \rightarrow X^1\Sigma^+$ laser induced fluorescence (LIF) spectra. In many LIF progressions the collision-induced satellite rotational lines were observed thus increasing the amount of term values and allowing to estimate the Λ-doubling effect in the $(4)^1\Pi$ state. The Direct-Potential-Fit (DPF) of experimental term values of 777 rovibronic levels of both ^{85}RbCs and ^{87}RbCs isotopologues has been performed by means of the robust weighted non-linear least squares method. The DPF analysis based on adiabatic approximation and analytical Expanded Morse Oscillator potential revealed numerous regular shifts in the measured level positions. The spectroscopic studies of the $(4)^1\Pi$ state were supported by the electronic structure calculations including the potential energy curves of the singlet and triplet states manifold and spin-allowed transition dipole moments. The subsequent estimates of radiative lifetimes and corresponding vibronic branching ratios elucidated a dominant contribution of the $(4)^1\Pi \rightarrow A \sim b$ channel into the total radiative decay of the $(4)^1\Pi$ state. The relative intensity distributions simulated for $(4)^1\Pi \rightarrow X^1\Sigma^+$ LIF progressions agree well with their observed counterparts even for the profoundly shifted levels of the entirely perturbed $(4)^1\Pi$ state. To get an insight into the origin of the intramolecular perturbations the relevant spin-orbit and L-uncoupling electronic matrix elements were evaluated.

PACS numbers: 33.20.Kf Visible spectra; 33.70.Ca Oscillator and band strengths, lifetimes, transition moments, and Franck-Condon factors; 33.80.Ps Optical cooling of the molecules; 31.15.ae Electronic structure and bonding characteristics; 31.15.aj Relativistic corrections, spin-orbit effects, fine structure

I. INTRODUCTION

The heteronuclear RbCs molecule became a focus of spectroscopic studies due to a rapid development of producing ultra-cold polar alkali diatomics, see [1–5] and references therein. An issue of particular experimental complexity is connected with a transfer from weakly bound triplet $a(1)^3\Sigma^+$ level, in which the molecules are created from the colliding ultracold atoms at long-range internuclear distances to their deeply bound vibronic level of the singlet $X^1\Sigma^+$ ground state. An alternative method was applied in Ref. [3], where RbCs molecules in $v'' = 0$ level of the $X^1\Sigma^+$ state have been formed via short-range photoassociation through the deeply bound mixed $(2)^3\Pi$ state. Since in both methods the transfer processes are realized via optical transitions, the information of energy and radiative properties of excited states of mixed singlet-triplet nature might broaden the possibilities of efficient optical paths. Though the quantum chemistry calculations of excited electronic states of RbCs were performed for a wide range of energies, see [6–9], the existing experiment based information on their potential energy curves (PECs) is still quite restricted. As far as highly excited states approaching the asymptotic limit Rb(5^2S) + Cs(5^2D) or higher are concerned, see Fig. 1, one can mention the molecular constants and RKR potentials for $(4,5)^1\Pi$ and $(7)^1\Sigma^+$ states obtained from fragmentary data on term values in Ref. [10]. Applying high-resolution resonance-enhanced two-photon ionization (RE2PI) spectroscopy to a molecular beam made it possible to study $(4-6)^1\Sigma^+$, $(3)^1\Pi$, and $(4)^3\Pi$ states, though including only the lowest rotational levels, see [11–14]. A detailed study of the $(4)^1\Sigma^+$ state that included modelling of prospective optical cycles for producing ground state ultra-cold species was performed in Ref. [15]. In our recent work [16] we studied the $(3)^1\Pi$ state of RbCs converging to the Rb(5^2S) + Cs(5^2D) asymptotic limit of separated atoms at about 18 400 cm^{-1}, as well as the $(5)^1\Sigma^+$ state converging to the Rb(5^2S) + Cs(7^2S) at about 22 400 cm^{-1}.

The present paper addresses the next excited $(4)^1\Pi$ state of the RbCs molecule converging to the Rb(4^2D) + Cs(6^2S) asymptotic limit at about 23 200 cm^{-1}. From the point of testing the *ab initio* calculation approaches, it is of additional interest to have more experiment-based information on the electronic states, which are converging to asymptotic limits that include a *d*-shell alkali atom. Indeed, though spin-orbit splitting for Rb(4^2D) is small, it still plays a profound role due to strong con-

* ferber@latnet.lv
† avstol@phys.chem.msu.ru

figuration interaction with lower states converging to the asymptote that includes the Rb(5^2P) limit. The only currently existing data on the $(4)^1\Pi$ state can be found in Ref. [10], where 38 experimental term values have been obtained from high-resolution Fourier-transform (FT) spectra of laser-induced fluorescence (LIF) excited by visible lines of Ar^+ laser. There is a dense manifold of different symmetry states in the energy range of the $(4)^1\Pi$ state. Hence, the latter is expected to be subject to numerous perturbations, as it was observed for the $(4)^1\Pi$ state in KCs, see [17]. Therefore we will refer to the $(4)^1\Pi$ state of RbCs as an entirely perturbed.

In present study we extended spectroscopic information on the $(4)^1\Pi$ state significantly by recording high-resolution FT spectra of LIF excited by two-step laser excitation. In performing the experiments, a particular $(4)^1\Pi(v', J')$ rovibronic level was reached via an intermediate level of fully mixed singlet-triplet $A^1\Sigma^+ \sim b^3\Pi$ complex, which has been comprehensively studied in Ref. [18]. This made it possible to predict with sufficient accuracy the required wave numbers of the first step of $(4)^1\Pi(v', J' = J; J \pm 1) \leftarrow A \sim b(E_{A\sim b}, J = J'' \pm 1) \leftarrow X^1\Sigma^+(v'', J'')$ excitation. The experimental term values were included into a Direct-Potential-Fit (DPF) analysis applying the robust weighted non-linear least squares method [19] and the fully analytical Expanded Morse Oscillator (EMO) potential [20]. The obtained EMO PEC was additionally validated by comparing experimental LIF intensity distributions with the ones derived from the empirical potential. For this purpose, the *ab initio* electronic structure calculations have been performed for the related states, along with estimates of radiative lifetimes and vibronic branching ratios. In addition, it appeared possible to experimentally determine the Λ-splitting energies Δ_{ef} and relevant q-factor as well as to compare the latter with a calculated value.

II. EXPERIMENT

Two-step excitation of the $(4)^1\Pi$ state of RbCs, see Fig. 1 was realized by two Ti-Sapphire lasers MBR110 (Coherent). The singlet-triplet $A^1\Sigma^+ \sim b^3\Pi$ complex served as intermediate state. Two copropagating laser beams were overlapped in the central part of the linear heat-pipe tube with rubidium and cesium metals operating at 300 °C. The heat-pipe was filled with Ar buffer gas at about 2 mbar pressure. The laser power variated from experiment to experiment, typically being within 300 – 500 mW for both lasers. The LIF spectra were recorded by FT spectrometer Bruker IFS 125HR at instrumental resolution 0.03 cm^{-1}. A photomultiplier tube (PMT) was used to detect the spectra in the range from 10 000 cm^{-1} to 22 000 cm^{-1}. The laser frequency needed to excite in the first step a particular $A^1\Sigma^+ \sim b^3\Pi(E_{A\sim b}, J) \leftarrow X^1\Sigma^+(v'', J'')$ transition was determined from calculated term values $E_{A\sim b}$ of the $A^1\Sigma^+ \sim b^3\Pi$ complex, which, according to Refs. [16, 18],

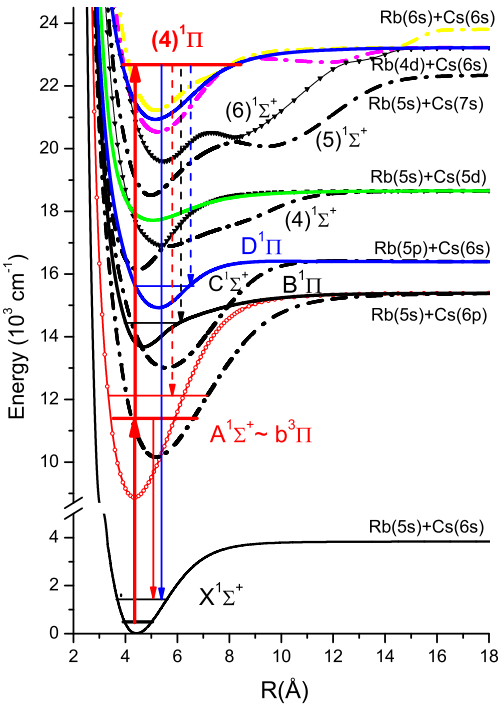

FIG. 1. (Color online) Based on Ref. [6] schema of the singlet states manifold of the RbCs molecule involved in the consideration. The solid vertical arrows show the two-step laser excitation of the $(4)^1\Pi$ state through an intermediate level of the singlet-triplet $A^1\Sigma^+ \sim b^3\Pi$ complex, as well as the observed LIF transitions. The dashed arrows denote the dominant radiative decay channels of the $(4)^1\Pi$ state.

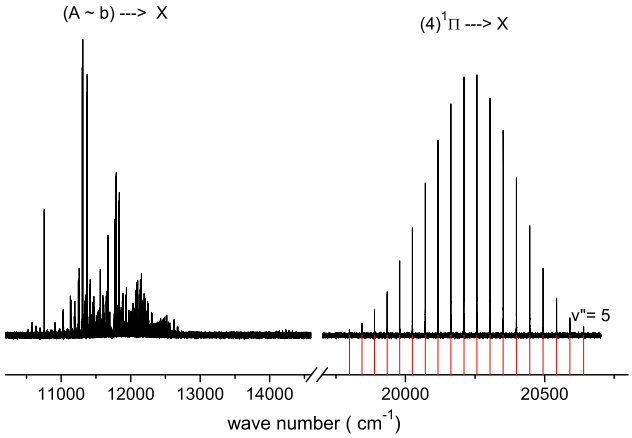

FIG. 2. (Color online) Right side: example of LIF spectrum (Q - progression) representing two-step excitation of the $(4)^1\Pi$ state by transitions $(4)^1\Pi$ ($v' = 0, J' = 10f, E' =$ 20 913.462 cm^{-1}) $\leftarrow A^1\Sigma^+ \sim b^3\Pi(E_{A\sim b} =$ 10 160.215 cm^{-1}, $J = 10) \leftarrow X^1\Sigma^+(v'' = 4, J'' = 9)$; laser frequencies are $\nu_{L1} =$ 9935.917 cm^{-1} and ν_{L2}=10 753.243 cm^{-1}. Left side: a fragment of the respective $A \sim b \rightarrow X$ LIF spectrum.

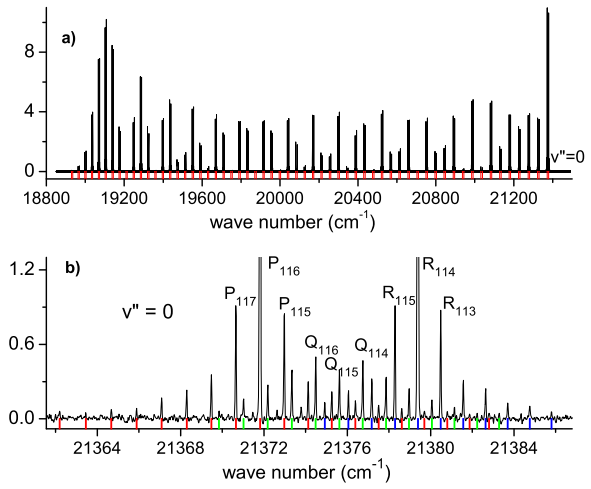

FIG. 3. (Color online) Example of LIF spectrum (P, R progression) representing two-step one-color excitation with laser frequency $\nu_{L1} \equiv \nu_{L2}$=10 683.992 cm^{-1} in transitions $(4)^1\Pi(v' = 19, J' = 115e, E' = 21\,620.507$ cm$^{-1}) \leftarrow A^1\Sigma^+ \sim b^3\Pi$ ($E_{A\sim b} = 10\,936.519$ cm^{-1}, $J = 116) \leftarrow X^1\Sigma^+(v'' = 0, J'' = 117)$: (**a**) entire spectrum; (**b**) zoomed fragment with transitions to $v'' = 0$ with satellite lines due to collisional population of neighbor rotational levels of the upper state of both e/f parity; red, blue, and green bars below the spectrum mark P, R and Q lines, respectively. Indices denote the J'' value of the X-state.

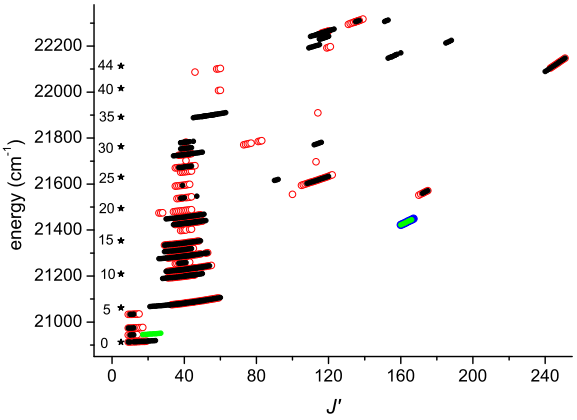

FIG. 4. (Color online) Data field of experimentally observed $(4)^1\Pi$ state rovibrational levels as dependent on J': red empty circles denote e-component of the ^{85}RbCs isotopologue, black points denote f-component of the ^{85}RbCs, green solid circles denote f-component of the ^{87}RbCs isotopologue, blue solid circles e-component of the ^{87}RbCs isotopologue; column with black stars denotes term values of the ^{85}RbCs isotopologue predicted with the present mass-invariant EMO potential for $J' = 5$.

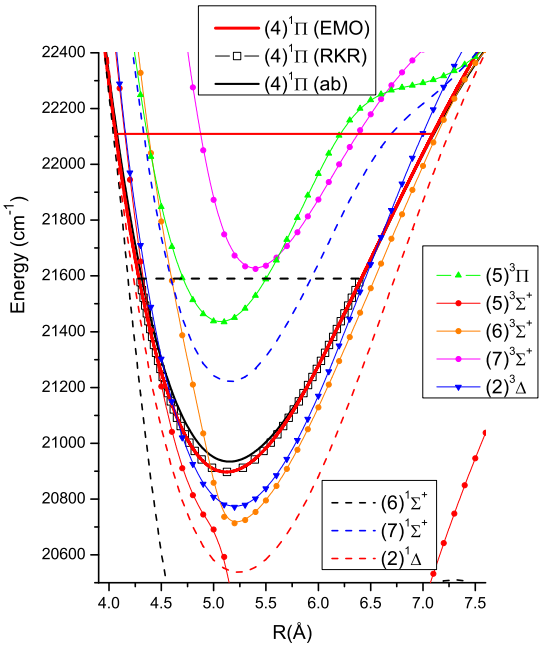

FIG. 5. (Color online) Present calculated difference-based potentials of the $(4)^1\Pi$ state and of the states, which are presumably responsible for both local and regular perturbations observed in the $(4)^1\Pi$ state. Present EMO PEC of the $(4)^1\Pi$ state is marked by solid red line, RKR potential from Ref. [10] is marked by open squares, red horizontal line denotes the experiment-based region of the present EMO PEC, while the dashed black horizontal line refers to the RKR potential [10].

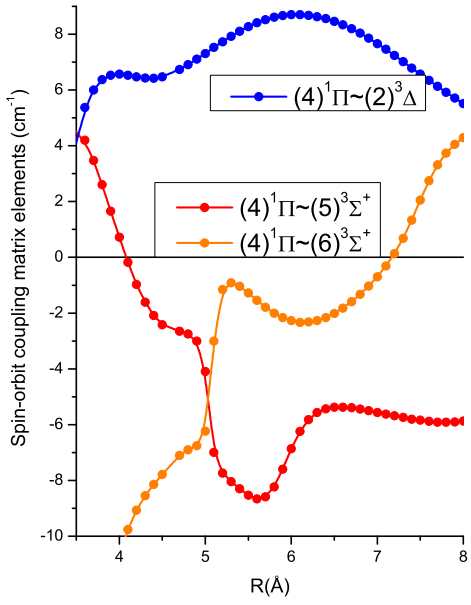

FIG. 6. (Color online) The *ab initio* spin-orbit coupling matrix element calculated between the singlet $(4)^1\Pi$ and triplet $(2)^3\Delta$ and $(5,6)^3\Sigma^+$ states of the RbCs molecule.

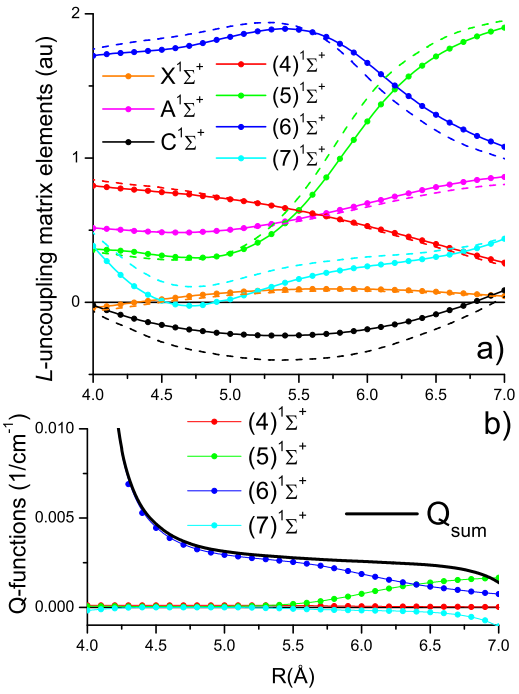

FIG. 7. (Color online) (**a**) The *ab initio* L-uncoupling electronic matrix elements of the RbCs molecule evaluated between the $(4)^1\Pi$ state and the $(1-7)^1\Sigma^+$ states. The dashed lines denote the previous results obtained in the framework of multi-partition perturbation theory calculation in Ref. [34]; (**b**) The partial contribution of the $(4-7)^1\Sigma^+$ states into the sum-over-states $Q(R)$-function as defined by Eq. (7).

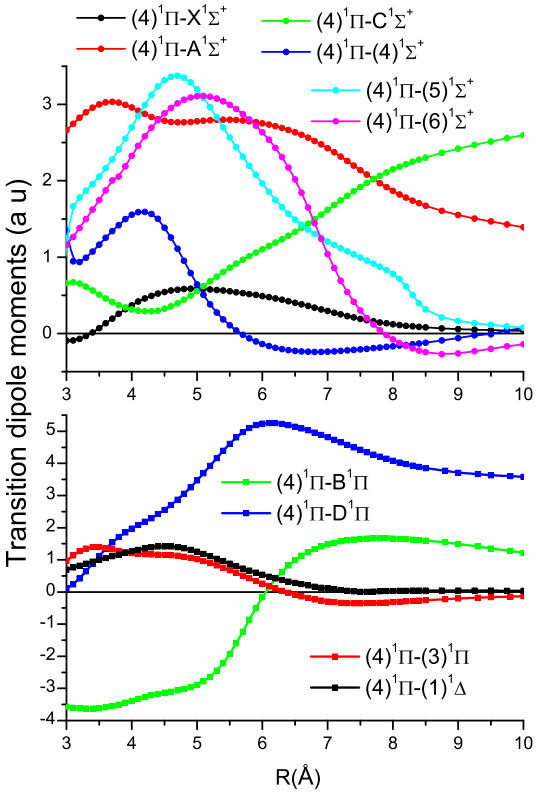

FIG. 8. (Color online) The *ab initio* electronic transition dipole moments obtained between the $(4)^1\Pi$ state and the $(1-6)^1\Sigma^+$, $(1-3)^1\Pi$, and $(1)^1\Delta$ states of the RbCs molecule.

can be predicted with experimental accuracy about 0.01 cm^{-1}. The ground $X^1\Sigma^+(v'', J'')$ level energies were calculated using the empirical PEC from Ref. [21].

The $A \sim b \rightarrow X$ LIF spectra in the range 6000−12 000 cm^{-1} were recorded and analyzed in order to find the optimal $A \sim b(E_{A\sim b}, J) \leftarrow X^1\Sigma^+(v'', J'')$ first step transition and to fine-tune the respective laser frequency. In this range the InGaAs diode was used for the infrared LIF detection.

At fixed first laser frequency ν_{L1}, the second laser was tuned over the range of $(4)^1\Pi \leftarrow A \sim b$ absorption bands, which were estimated using the Dunham molecular constants of the $(4)^1\Pi$ state from Ref. [10]. The appearance of two-step excitation was monitored by observation the $(4)^1\Pi \rightarrow X$ LIF signal in the range around 20 000 cm^{-1} in the Preview Mode of the FT spectrometer. To catch a weaker two-step excitation, the observation of illuminating area inside the heat pipe by eye through a blue filter was useful. In Fig. 2 the LIF spectrum is shown, which demonstrates a two-step excitation of the $(4)^1\Pi(v' = 0)$ level with a characteristic single maximum in $(4)^1\Pi(v' = 0) \rightarrow X^1\Sigma^+(v'')$ LIF intensity distribution (see the right side of the Figure).

According to the plan of the experiment we excited in the first step rotational levels of the $A \sim b$ complex with $J = 10$ and 40 of the ^{85}RbCs molecule. Hence, the observed rotational levels of the $(4)^1\Pi$ state in the second step excitation of P,R and Q transitions are possessing $J' = 9 - 11$ and $39 - 41$. However, LIF from a number of the $(4)^1\Pi$ levels with other J' values was also observed due to accidental resonances in the $A \sim b \leftarrow X$ and $(4)^1\Pi \leftarrow A \sim b$ transitions for the used frequencies of both lasers. In several cases two-step one-color excitation was observed. Moreover, as later analysis had shown, in some cases the laser nominated for the second step actually worked in the first step, and vice versa. Overall about 50 LIF spectra containing $(4)^1\Pi \rightarrow X^1\Sigma^+$ transition were recorded. Two progressions belonging to the ^{87}RbCs isotopologue were also assigned.

III. ANALYSIS OF SPECTRA

Assignment of LIF progressions $(4)^1\Pi \rightarrow X^1\Sigma^+$ was straightforward based on highly accurate vibrational and rotational differences of the ground X-state [21]. Due to the presence of Ar buffer gas in the heat-pipe many satellite lines from collisionally populated neighbouring

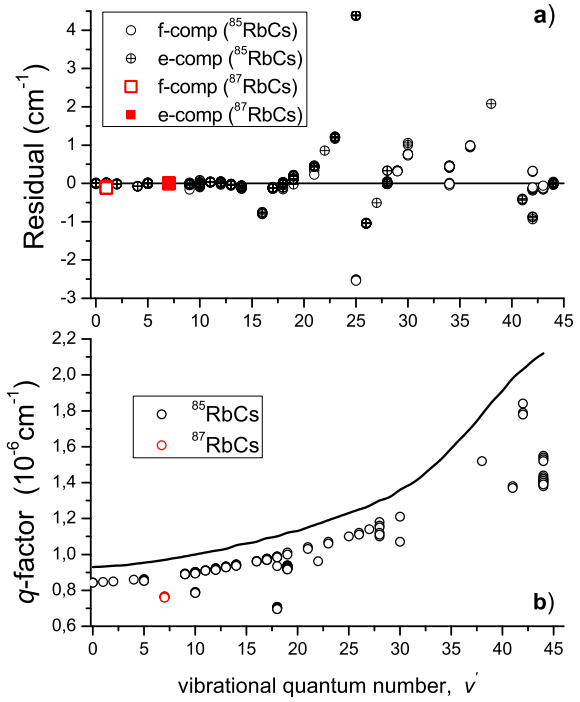

FIG. 9. (Color online) (**a**) Differences between experimental and calculated by the present EMO PEC rovibronic term values of the RbCs $(4)^1\Pi$ state as dependent on vibrational quantum number v'. (**b**) Empty circles represent the empirical $q_{v'}$-factors obtained during the DPF analysis based on EMO potential (5), the fixed *ab initio* $Q(R)$ function (7), and the fitted parameter $s = 0.908$; solid line represents the theoretical $q_{v'}$-values predicted due to the approximate sum rule (8) for $J' = 1$ levels of the ^{85}RbCs isotopologue using the constrained $s \equiv 1$ parameter.

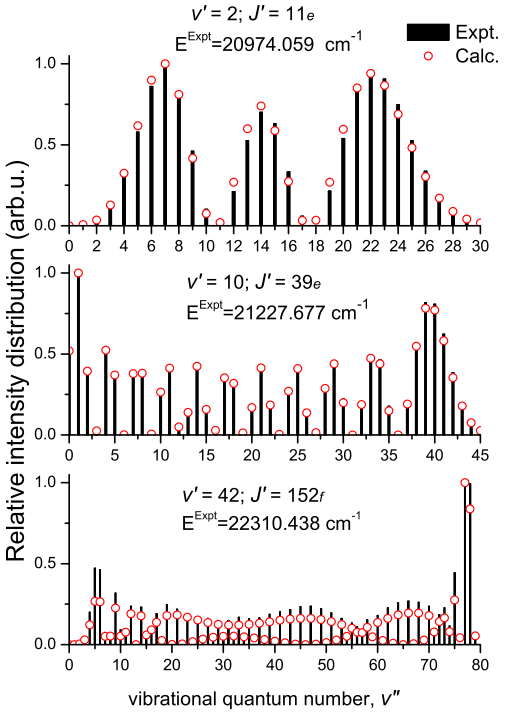

FIG. 10. (Color online) Comparison of experimental and calculated relative intensity distributions in the full $(4)^1\Pi(v', J') \rightarrow X^1\Sigma^+(v'')$ LIF progressions starting from the weakly perturbed vibrational levels v' =2, 10, and 42 of the $(4)^1\Pi$ state of the ^{85}RbCs isotopologue; the respective residuals between the experimental and calculated term values are: -0.009 cm^{-1}, 0.01 cm^{-1}, and 0.332 cm^{-1}.

rotational levels of both parity where observed around the strong lines, therefore much more term values of rovibronic levels of the $(4)^1\Pi$ state could be obtained. This is demonstrated in Fig. 3 by a P,R LIF progression recorded at two-step one-color excitation with laser frequency 10 683.992 cm^{-1}. In the first step laser excites transition $A^1\Sigma^+ \sim b^3\Pi$ ($E_{A\sim b}$ = 10 936.519 cm^{-1}, $J = 116$) $\leftarrow X^1\Sigma^+(v'' = 0, J'' = 117)$, and in the second step it excites the $(4)^1\Pi(v' = 19, J' = 115e)$ level with energy E' = 21 620.507 cm^{-1}. In Fig. 3b a zoomed fragment is shown with transitions to $v''_X = 0$. Along with P and R satellite lines originating from e-parity levels, the Q lines from f-parity levels can be clearly distinguished. The energy difference between e and f components of a particular rovibrational level v', J' allows determination of Λ-splitting Δ_{ef} and a respective experimental q-factor:

$$\Delta_{ef} \equiv E^e_{v'J'} - E^f_{v'J'} = q^{expt}_{v'}[J'(J'+1) - 1]. \quad (1)$$

However, the observed energy differences are very small and in most cases comparable with an accuracy of line position determination being about 0.003 - 0.005 cm^{-1}. A crude estimate of the Δ_{ef}-splitting for high rotational levels yielded the $q^{expt}_{v'}$-value of about $+1.0 \times 10^{-6}$ cm^{-1}.

It should be noted that the intensity of Q_{115} line, see Fig.3b, is by about 20% less than that of Q lines from neighbouring rotational levels Q_{114} and Q_{116}. It means that collisional transfer of population from an optically excited rotational level J' with a particular parity to an opposite parity component of the same rotational level is less efficient than that of the collisional transfer to the neighbouring $(J' \pm 1)$ rotational levels. This effect took place in all cases when satellite lines from levels of both parities could be clearly distinguished.

The resulting data field of the observed rovibronic $(4)^1\Pi$ state levels of both ^{85}RbCs and ^{87}RbCs isotopologues is presented in Fig. 4. It contains averaged over different measurements term values of 419 f and 332 e levels for ^{85}RbCs, as well as 18 f and 8 e levels for ^{87}RbCs. The data set spans over vibrational levels v' from 0 to 44 and rotational levels J' from 9 to 251.

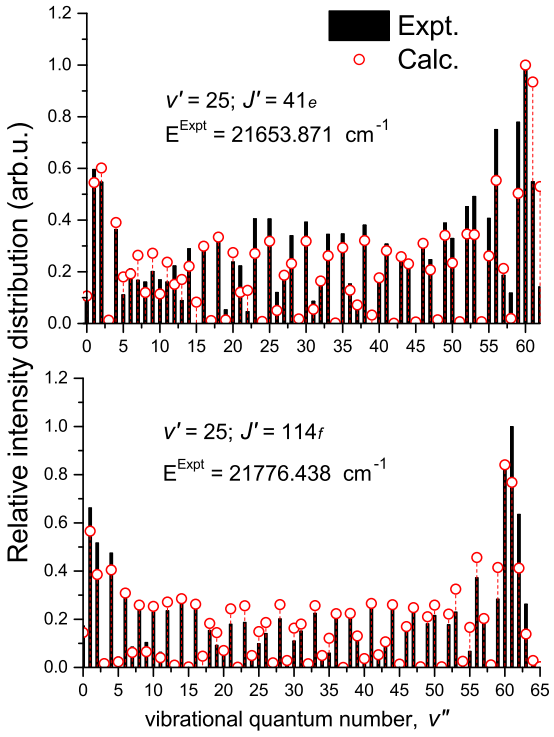

FIG. 11. (Color online) Comparison of experimental and calculated relative intensity distributions in full $(4)^1\Pi(v' = 25; J') \rightarrow X^1\Sigma^+(v'')$ LIF progressions starting from locally perturbed $J' = 41$ and 114 rovibronic levels of the ^{85}RbCs isotopologue; the respective residuals between the experimental and calculated term values are: 4.385 cm^{-1} and –2.532 cm^{-1} .

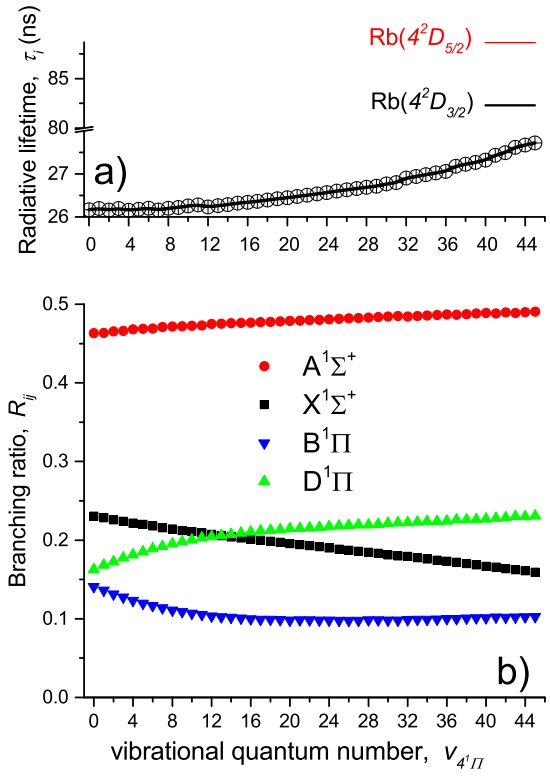

FIG. 12. (Color online) Radiative lifetimes (**a**) and vibronic branching ratios (**b**) of vibrational levels v' of the ^{85}RbCs $(4)^1\Pi$ state evaluated using the present EMO PEC for the upper state as well as the corresponding *ab initio* ETDM functions and adiabatic PECs evaluated for the lower-lying singlet states manifold by Eq. (11). The lifetimes of related atomic levels are presented in (**a**) by short solid lines.

IV. ELECTRONIC STRUCTURE CALCULATIONS

The details of the present *ab initio* quasi-relativistic calculation can be found elsewhere [22]. Briefly, the inner core shell of both rubidium and cesium atoms was replaced by the shape-consistent non-empirical effective core potentials (ECPs) [23], leaving nine outer shells (eight sub-valence plus one valence) electrons for explicit correlation treatment. The molecular orbitals were obtained from the solutions of the state-averaged complete active space self-consistent field (SA-CASSCF) problem for all 18 electrons on the lowest $(1 - 10)^{1,3}\Sigma^+$, $(1 - 6)^{1,3}\Pi$ and $(1 - 2)^{1,3}\Delta$ electronic states taken with equal weights [24]. The dynamical correlation energy was estimated by internally contracted multi-reference configuration interaction (MRCI) method [25]. The MRCI procedure included all single and double excitations in the large $14a_1$, $8b_1$, $8b_1$, $2a_2$ (in the C_{2v} symmetry) active space, however, it was applied for only two valence electrons keeping the 16 sub-valence electrons frozen.

TABLE I. The static electric dipole polarizabilities [28], α_c^+, and the exponential cut-off parameters, k_c, which are used to build the CPP potentials of Rb and Cs atoms. Both α_c^+ and k_c are given in *au*.

Atom	α_c^+	k_c
Rb	9.096	0.350
Cs	15.687	0.278

The core-polarization potentials (CPPs) [26] of both atoms were exploited to account for the core-valence correlation effect implicitly. The Mueller-Meyer [27] damping functions are implemented in the present CPP construction. The required static dipole polarizabilities of the atomic cation, α_c^+, were borrowed from Ref. [28] while the initial sets of the exponential cut-off parameter k_c (see Table I) were adjusted to reproduce experimental atomic energies [29] of the excited Rb(4^2D) and Cs(7^2S) states, respectively.

The adiabatic PECs of both singlet and triplet states manifold of the RbCs molecule were calculated in the basis of spin-averaged electronic wavefunctions corresponding to pure (**a**) Hund's coupling case [30], along with the singlet-singlet $(4)^1\Pi - (1-7)^1\Sigma^+; (1-3)^1\Pi; (1-2)^1\Delta$ electronic transition dipole moment (ETDM) functions $d_{ij}^{ab}(R)$. To clarify the origin of the Λ-doubling effect in the $(4)^1\Pi$ state the L-uncoupling electronic matrix elements $L_{ij}^{ab}(R)$ between the $(4)^1\Pi$ and $(1-7)^1\Sigma^+$ and $(1-2)^1\Delta$ states were evaluated as well.

According to the selection rule $\Delta\Omega = 0$ ($\Omega = \Lambda+\Sigma$) the singlet-triplet $(4)^1\Pi-(1-4)^3\Pi; (1-7)^3\Sigma^+; (1-2)^3\Delta$ spin-orbit coupling (SOC) matrix elements $\xi_{ij}^{so}(R)$ between the individual quasi-relativistic $|S, \Sigma, \Lambda\rangle$ eigenstates were evaluated by means of the corresponding SO part of the present ECP pseudopotentials. All calculations were performed in the wide range of the internuclear distance using the MOLPRO program suit [31].

V. DIRECT-POTENTIAL-FIT PROCEDURE

A DPF analysis of the entirely perturbed $(4)^1\Pi$ state has been performed in the framework of the robust weighted non-linear least squares procedure [19] in order to diminish the undesirable impact of outliers caused by local perturbations. To constrain the modeling potential $U^{emp}(R)$ outside the experimental data region the corresponding χ^2 function included the difference-based PEC $U^*(R_i)$ (see Eq. (12) in Section VII A) of the $(4)^1\Pi$ state as well:

$$\chi^2 = \sum_{i=1}^{N_{expt}} \frac{(\delta_i^{expt})^2}{(\sigma_i^{expt})^2 + (\delta_i^{expt})^2/3} + w \sum_{i=1}^{N_{ab}} \left(\frac{\delta_i^{ab}}{\sigma_i^{ab}}\right)^2, \quad (2)$$

$$\delta_i^{expt} = E_i^{expt} - E_i^{calc}; \quad \delta_i^{ab} = U^*(R_i) - U^{emp}(R_i),$$

where the empirical term values E_i^{calc} were calculated from the iterative numerical solution of the radial equation

$$\left(-\frac{\hbar^2 d^2}{2\mu dR^2} + U^{eff}(R) - E_i^{calc}\right)|v_i^J\rangle = 0 \quad (3)$$

with the effective interatomic potential $U^{eff}(R)$, which accounts for the Λ-doubling effect in the degenerate $^1\Pi$ state explicitly:

$$U^{eff} = U^{emp} + B[1 + sQB][J(J+1) - 1], \quad (4)$$

where $B(R) \equiv \frac{\hbar^2}{2\mu R^2}$ and $U^{emp}(R) = T_{dis} - D_e + U^{EMO}$ is the mass-invariant empirical potential taken in the fully analytical EMO form [20]

$$U^{EMO} = D_e \left(1 - \exp[-\beta(R - R_e)]\right)^2, \quad (5)$$

where D_e is the the well depth, R_e is the equilibrium distance and the coefficient β

$$\beta(R) = \sum_{i=0}^{N} \beta_i \left[y_p\right]^i; \quad y_p(R) = \frac{R^p - R_{ref}^p}{R^p + R_{ref}^p} \quad (6)$$

is the polynomial function of the reduced radial coordinate y_p, while R_{ref} is the reference distance and p is the integer parameter.

The dimensionless scaling parameter s in Eq. (4) is equal to zero for the f-parity levels while it is considered as an adjusted parameter for the regularly perturbed levels of the e-component. $Q(R)$ is the non-adiabatic correction function computed in advance by means of the *ab initio* adiabatic potentials $U_i^{ab}(R)$ and L-uncoupling electronic matrix elements $L_{ij}^{ab}(R)$ between the $(4)^1\Pi$ and $(1-7)^1\Sigma^+$ states obtained in Section IV:

$$Q(R) = 2 \sum_{^1\Sigma^+} \frac{|L^{ab}_{^1\Pi - ^1\Sigma^+}|^2}{U^{ab}_{^1\Pi} - U^{ab}_{^1\Sigma^+}}. \quad (7)$$

It should be noticed that according to the approximate sum rule [32] both $Q(R)$-function and a scaling parameter s are related to the corresponding q-factors as

$$q_v^{calc} \approx s\langle v^J|BQB|v^J\rangle. \quad (8)$$

The uncertainties of experimental data σ_i^{expt} were taken equal to 0.005 cm^{-1} for all term values involved. The required uncertainties σ_i^{ab} in the *ab initio* difference-based potential $U^*(R)$ were estimated by a comparison with its previous theoretical counterparts [6, 9, 33] (see Table II). The weighting factor w in Eq. (2) was selected to reach a proper balance between the contribution of experimental and theoretical data sets into the total χ^2-value.

VI. ESTIMATE OF RADIATIVE PROPERTIES

The reliability of the performed DPF analysis, which has been accomplished under the conventional adiabatic approximation using only the energy data set, was additionally tested by a comparison of the simulated relative intensity distributions in the long $(4)^1\Pi \rightarrow X^1\Sigma^+$ LIF progressions with their experimental counterparts. The corresponding rovibronic transition probabilities from rovibrational $v^{J'}$ levels of the $(4)^1\Pi$ state to rovibrational levels $v^{J''}$ of the ground $X^1\Sigma^+$ state were calculated as

$$I_{ij}^{calc} \sim \nu_{ij}^4 |\langle v^{J'}|d_{ij}^{ab}|v^{J''}\rangle|^2, \quad (9)$$
$$\nu_{ij} = E_{v^{J'}} - E_{v^{J''}},$$

where $i \in (4)^1\Pi; j \in X^1\Sigma^+$, rovibrational eigenvalues $E_{v^{J'}}$ and eigenfunctions $|v^{J'}\rangle$ of the upper state were obtained by the solution of radial equation (3) with the present EMO potential, while the empirical potential U_X^{emp} was borrowed from Ref. [21] to calculate the corresponding $E_{v^{J''}}$ and $|v^{J''}\rangle$ of the ground X-state. Here, $d_{ij}^{ab}(R)$ is the *ab initio* ETDM function obtained for the $(4)^1\Pi \rightarrow X^1\Sigma^+$ transition in Section IV.

The spin-allowed ETDM functions $d_{ij}^{ab}(R)$ derived in the Section IV between the $(4)^1\Pi$ state and lower-lying states manifold j denoting $(1-4)^1\Sigma^+$ and $(1-2)^1\Pi$ (see

Fig. 1) were used to estimate radiative lifetimes τ_i and vibronic branching ratios R_{ij} of vibrational levels of the $(4)^1\Pi$ state:

$$\frac{1}{\tau_i^{calc}} \approx \frac{8\pi^2}{3\hbar\epsilon_0}\langle v^{J'}|\sum_j [\Delta U_{ij}^{ab}]^3[d_{ij}^{ab}]^2|v^{J'}\rangle, \quad (10)$$

$$R_{ij}^{calc} = \frac{8\pi^2}{3\hbar\epsilon_0}\langle v^{J'}|[\Delta U_{ij}^{ab}]^3[d_{ij}^{ab}]^2|v^{J'}\rangle \times \tau_i^{calc}, \quad (11)$$

where $\Delta U_{ij}^{ab} = U_i^{ab}(R) - U_j^{ab}(R)$ is the difference of the *ab initio* PECs. Here, the approximate sum rule [32] was used again to avoid summation over bound part and an integration over continuum part of the vibrational spectra of the lower states.

VII. RESULTS AND DISCUSSION

A. *Ab initio* PECs, transition dipole moments, L-uncoupling and spin-orbit coupling matrix elements

All originally calculated adiabatic potentials $U_i^{ab}(R)$ for the $(1-7)^{1,3}\Sigma^+$, $(1-4)^{1,3}\Pi$ and $(1-2)^{1,3}\Delta$ states (except the ground X-state) were transformed to the relevant "difference-based" PECs $U_i^*(R)$ by means of the semi-empirical relation [34]

$$U_i^* = [U_i^{ab} - U_X^{ab}] + U_X^{emp} \quad (12)$$

in order to diminish a basis set superposition error (BSSE) in the originally calculated *ab initio* PECs $U_i^{ab}(R)$ for the excited electronic states. $U_X^{emp}(R)$ is the highly accurate empirical PEC available for the ground $X^1\Sigma^+$ state [21] of RbCs in a wide R-range. The singlet-triplet states manifold located in vicinity of the $(4)^1\Pi$ state is depicted in Fig. 5. Equilibrium constants R_e and T_e obtained from present difference-based potential of the $(4)^1\Pi$ state are provided in Table II along with other sources. Note that the nearby lying triplet $(5,6)^3\Sigma^+$ and $(2)^3\Delta$ states intersect both repulsive and attractive walls of the $(4)^1\Pi$ state PEC.

The relevant spin-orbit coupling electronic matrix elements are shown in Fig. 6. The sharp R-dependence of the $(4)^1\Pi$ – $(5)^3\Sigma^+$ and $(4)^1\Pi$ – $(6)^3\Sigma^+$ SOC matrix elements observed near the point at $R_c \approx 5.1$ Å is attributed to the avoided crossing effect taking place between the adiabatic $(5)^3\Sigma^+$and $(6)^3\Sigma^+$ states (see Fig. 5).

The L-uncoupling matrix elements between the $(4)^1\Pi$ and the first seven $(1-7)^1\Sigma^+$ states are depicted in Fig. 7a. The present $L_{ij}^{ab}(R)$ functions are found to be very close to the previous results obtained in the framework of multi-partition perturbation theory (MPPT) in Ref. [34]. The fractional contributions of the individual $^1\Sigma^+$ states into the total sum (7) are shown in Fig. 7b. It can be seen that a dominant contribution into the Λ-doubling of the $(4)^1\Pi$ state is caused by the interaction with the $(6)^1\Sigma^+$ state, which crosses the repulsive wall of the $(4)^1\Pi$ state near the point at $R_c \approx 4.1$ Å (see Fig. 5), while the contribution of the $(7)^1\Sigma^+$ state is almost negligible.

TABLE II. Comparison of equilibrium distance R_e and electronic energy T_e values available for the $(4)^1\Pi$ state of the RbCs molecule. The theoretical results correspond to pure Hund's (**a**) coupling case. The abbreviation PW marks the present work.

Source	R_e (Å)	T_e (cm^{-1})
Experiment		
PW	5.119	20896.905
10	5.117	20896.952
Theory		
PW	5.15	20931
34	5.16	20959
8	5.13	20970
33	5.06	20977
6	5.08	21034
9	5.09	21294

The calculated spin-allowed singlet-singlet $(4)^1\Pi$ – $(1-6)^1\Sigma^+$, $(4)^1\Pi$ – $(1-3)^1\Pi$ and $(4)^1\Pi$ – $(1)^1\Delta$ ETDMs are presented in Fig. 8. Among them the $d_{ij}^{ab}(R)$ functions for $(4)^1\Pi$ – $(2)A^1\Sigma^+$ and $(4)^1\Pi$ – $(2)D^1\Pi$ transitions are predicted to be the strongest in intermediate internuclear distance range.

The *ab initio* PECs, ETDM functions, L-uncoupling and SOC matrix elements are available in the Supplemented Material [35] in a point-wise form.

B. Experimental term values, q-factors and the empirical PEC

The overall non-averaged $N_{expt} = 866$ experimental rovibronic term values E_i^{expt} assigned to both isotopologues and both e/f-components were simultaneously involved into the present DPF analysis. The resulting mass-invariant parameters of the EMO potential obtained for the RbCs $(4)^1\Pi$ state are given in Table III. The EMO potential is presented in Fig. 5. As expected, the lower part of the present EMO PEC is very close to the RKR potential constructed in Ref. [10], the latter however being reliable in more restricted energy region. The derived EMO PEC agrees well also with the present difference-based potential $U^*(R)$ and with most of previous *ab initio* results (see Table II).

The differences between experimental and fitted rovibronic termvalues, or the residuals, are represented in Fig. 9a as dependent on vibrational quantum number v'. The experimental and fitted term values along with residuals are available in the Supplemented Materials [35]. The significant residuals observed around $v' = 16$, 25, 30, 38, and 42 should apparently arise due to local non-adiabatic interactions with the $(2)^3\Delta$, $(5,6)^3\Sigma^+$, and $(6)^1\Sigma^+$ states. In particular, the largest energy shifts exceeding 4 cm^{-1} for $v' = 25$ seem to be attributed to

TABLE III. The resulting mass-invariant parameters of the empirical EMO potential (5) constructed for the RbCs $(4)^1\Pi$ state. Energies are given in cm^{-1}, the internuclear distance in Å and the polynomial coefficients β_i in 1/Å. The parameters T_{dis} = 23191.503 cm^{-1}, $p = 4$ and R_{ref} = 5.0 Å were fixed during the fit. The numbers are truncated up to six decimal digits, the full values are given in the supplementary material [35].

D_e	2294.598
R_e	5.119042
β_0	0.555711
β_1	0.034720
β_2	-0.221238
β_3	1.129969
β_4	3.753468
β_5	-6.477096
β_6	-20.401909
β_7	18.648820
β_8	51.312053
β_9	-23.267061
β_{10}	-58.915683
β_{11}	9.920143
β_{12}	25.000342

the pronounced SOC effect with the nearby triplet $(2)^3\Delta$ state (see Fig. 6). Unfortunately, a comprehensive deperturbation analysis of the $(4)^1\Pi$ state is strictly limited because of fragmentary spectroscopic data available.

The empirical $q_{v'}^{emp}$-factors obtained during the simultaneous DPF analysis of the experimental termvalues belonging to both e and f-components are presented in Fig. 9b. As expected, the fitted scaling parameter $s = 0.908$ involved in Eqs. (4) is slightly less than 1 since the estimated sum-over-states Q-function (7) obviously neglects the negative contributions of the higher-lying $(i > 7)^1\Sigma^+$ states. The $q_{v'}^{calc}$-values estimated for $J' = 1$ levels by means of the approximate sum rule (8) and constrained $s \equiv 1$ parameter are slightly higher than their empirical counterparts. It should be noted that present q-values agree quite well with the previous theoretical q-value $+0.8\times10^{-6}$ cm^{-1} reported in Ref. [34].

C. Intensity distributions, radiative lifetimes and vibronic branching ratios

The measured and simulated relative intensity distributions of full $(4)^1\Pi(v', J') \rightarrow X^1\Sigma^+(v'')$ LIF progressions starting from the weakly and pronouncedly perturbed vibrational levels of the $(4)^1\Pi$ state of ^{85}RbCs isotopologue are presented in Fig. 10 and Fig. 11, respectively. In the case of doublet progressions experimental intensity distributions of P- and R-branches were averaged while the corresponding theoretical intensities were obtained under the Q-branch ($J' = J''$) approximation. Overall a very good agreement between the experimental intensities and their calculated counterparts takes place for weakly perturbed levels. The agreement is satisfactory even for the markedly non-adiabatically shifted levels. The well-known Condon reflection principle is certainly valid for an intensity distribution observed from low vibrational levels ($v' = 2$ and 10) of the upper state since a number of maxima in the $I(v''_X)$ function is unambiguously equal to $v' - 1$. As it was expected for high vibrational levels (e.g. $v' = 42$) the so-called "interference structure" of LIF intensity distribution is observed.

The calculated τ_i and R_{ij} values of the $(4)^1\Pi$ state are depicted in Fig. 12. As is seen, the lifetime slowly increases as v' increases. The predicted τ-values are by about 10 and 2 times smaller than the τ-values calculated in Ref. [16] for the $(3)^1\Pi$ and $(5)^1\Sigma^+$ states, respectively. Furthermore, in contrast to the increasing τ-values of the $(4)^1\Pi$ state, the radiative lifetimes of both $(3)^1\Pi$ and $(5)^1\Sigma^+$ states are rapidly decreasing with growing v'.

As expected, the dominant decay channel of the$(4)^1\Pi$ state is the infrared (IR) transition to the $A \sim b$ complex. However, in contrast to the case of $(3)^1\Pi$ and $(5)^1\Sigma^+$ states [16], the decay rate to the ground $X^1\Sigma^+$ state is only two times smaller than to the $A \sim b$ complex, therefore the visible $(4)^1\Pi \rightarrow X^1\Sigma^+$ LIF could be easily observed. The contribution of the far IR $(4)^1\Pi \rightarrow B, D^1\Pi$ transitions is almost the same as of transitions to the ground state, the $(4)^1\Pi \rightarrow D^1\Pi$ channel being more efficient than the $(4)^1\Pi \rightarrow B^1\Pi$ channel.

VIII. CONCLUDING REMARKS

We performed a high resolution Fourier-transform spectroscopic study of the highly excited $(4)^1\Pi$ state of the RbCs molecule by applying two-step $(4)^1\Pi \leftarrow A^1\Sigma^+ \sim b^3\Pi \leftarrow X^1\Sigma^+$ optical excitation followed by observation of the collisionally enriched $(4)^1\Pi \rightarrow X^1\Sigma^+$ laser induced fluorescence spectra. The summary of two-step excitation transitions exploited in present experiment is provided in Supplemented Material [35]. The direct-potential-fit of experimental rovibronic term values determined in the interval $v' \in [0, 44], J' \in [9, 251]$ with uncertainty of 0.005 cm^{-1} has revealed a numerous shifts in the measured level positions with respect to their adiabatically (single state) fitted counterparts. In contrast to the term value positions, the relative intensity distributions simulated for the measured $(4)^1\Pi \rightarrow X^1\Sigma^+$ LIF progressions agree well with their experimental counterparts even for the profoundly perturbed levels of the upper state. The sum-over-states Λ-doubling factors estimated for the $(4)^1\Pi$ state support their experimental counterparts as well.

We believe that the derived energies and radiative properties of the entirely perturbed $(4)^1\Pi$ state of the RbCs molecule will facilitate its future usage as an intermediate state in multi-step laser induced population transfer to both lower (including the absolute ground state) and higher-lying states manifold. The present experimental and *ab initio* studies may serve as the first step to acquiring more abundant spectroscopic informa-

tion, which will make it possible to perform a comprehensive deperturbation analysis of the $(4)^1\Pi$ state along with the neighboring interacting states.

ACKNOWLEDGMENTS

Moscow team is grateful for the support by the RFBR grant No.16-03-00529a. Riga team acknowledges the support from the Latvian Science Council Grant LZP2018/5: "Determination of structural and dynamic properties of alkali diatomic molecules for quantum technology applications" and from the University of Latvia Base Funding No A5-AZ27; A.K. acknowledges the support from the Post-doctoral Grant No 1.1.1.2/16/I/001, proposal No 1.1.1.2/I/16/068.

.

[1] T. Takekoshi, L. Reichsöllner, A. Schindewolf, J. M. Hutson, C. R.Le Sueur, O. Dulieu, F. Ferlaino, R. Grimm, and H.-Ch. Nägerl, Phys. Rev. Lett. **113**, 205301 (2014).
[2] P. K. Molony, P. D. Gregory, Z. Ji, B. Lu, M. P. Köppinger, C. Ruth Le Sueur, C. L. Blackley, J. M. Hutson, and S. L. Cornish, Phys. Rev. Lett. **113**, 255301 (2014).
[3] C. D. Bruzewicz, M. Gustavsson, T. Shimasaki, and D. DeMille, New J. Phys. **16**, 023018 (2014).
[4] T. Shimasaki, J.-T. Kim, and D. DeMille , Chem. Phys. Chem. **17**, 1 (2016).
[5] G. Quéméner and P. S. Julienne, Chem. Rev. **112**, 4949 (2012).
[6] A. R. Allouche, M. Korek, K. Fakherddin, A. Chaalan, M. Dagher, F. Taher, and M. Aubert-Frecon, J. Phys. B **33**, 2307 (2000).
[7] H. Fahs, A.R. Allouche, M. Korek, and M. Aubert-Frecon, J. Phys. B: At. Mo. Opt. Phys., **35**, 1501 (2002).
[8] H. Souissi, S. Jellali, Ch. Maha, H. Habli, B. Oujia, and F. H. Gadéa, J. Quant. Spectrosc. Radiat. Transfer, **200**, 173 (2017).
[9] I. S. Lim, W. C. Lee, Y. S. Lee, and G.-H. Jeung, J. Chem. Phys. **124**, 234307 (2006).
[10] T. Gustavsson, C. Amiot, and J. Verges, Mol. Phys. **64**, 293 (1988).
[11] B. Kim and K. Yoshihara, Chem. Phys. Lett. **212**, 271 (1993).
[12] B. Kim and K. Yoshihara, J. Chem. Phys. **100**, 1849 (1994).
[13] Y. Yoon, Y. Lee, T. Kim, J. S. Ahn, Y. Jung, B. Kim, and S. Lee, J. Chem. Phys. **114**, 8926 (2001).
[14] Y. Lee, Y. Yoon, S. Lee, and B. Kim, J. Phys. Chem. A **113**, 12187 (2009).
[15] V. Zuters, O. Docenko, M. Tamanis, R. Ferber, V. V. Meshkov, E. A. Pazyuk,and A. V. Stolyarov, Phys. Rev. A **87**, 022504 (2013).
[16] K. Alps, A. Kruzins, O. Nikolayeva, M. Tamanis, R. Ferber, E. A. Pazyuk, and A. V. Stolyarov, Phys. Rev. A **96**, 022510 (2017).
[17] J. Szczepkowski, A. Grochola, W. Jastrzebski, P. Kowalczyk, Chem. Phys. Lett., **576**, 10 (2013).
[18] A. Kruzins, K. Alps, O. Docenko, I. Klincare, M. Tamanis, R. Ferber, E. A. Pazyuk, and A. V. Stolyarov, J. Chem. Phys. **141**, 184309 (2014).
[19] J. K. G. Watson, J. Mol. Spectrosc. **219**, 326 – 328 (2003).
[20] R. J. LeRoy and A. Pashov, J. Quant. Spectrosc. Radiat. Transfer, **186**, 210 (2016).
[21] O. Docenko, M. Tamanis, R. Ferber, H. Knöckel, and E. Tiemann, Phys. Rev. A **83**, 052519 (2011).
[22] E. A. Pazyuk, A. V. Zaitsevskii, A. V. Stolyarov, M. Tamanis, and R. Ferber, Russ. Chem. Rev., **84** (10), 1001 (2015).
[23] R. B. Ross, J.M. Powers, T. Atashroo, W. C. Ermler, L. A. LaJohn, and P. A. Christiansen, J. Chem. Phys. **93**, 6654 (1990).
[24] H.-J. Werner and P. J. Knowles, J. Chem. Phys. **82**, 5053 (1985).
[25] P. J. Knowles and H.-J. Werner, Theor. Chim. Acta **84**, 95 (1992).
[26] P. Fuentealba, H. Stoll, L. V. Szentpaly, P. Schwerdtfeger, and H. Preuss, J. Phys. B **16**, L323 (1983).
[27] W. Müller, J. Flesch, and W. Meyer, J. Chem. Phys. **80**, 3297 (1984).
[28] J. Mitroy, M. S. Safronova, and C. W. Clark, J. Phys. B **43**, 202001 (2010).
[29] NIST Atomic data base; *http://physics.nist.gov/*
[30] R.W. Field and H. Lefebvre-Brion, *The Spectra and Dynamics of Diatomic Molecules*, Elsevier, Amsterdam, 2004.
[31] H.-J. Werner, P. J. Knowles, G. Knizia, F. R. Manby, M. Schütz *et al.*, *MOLPRO, version 2010.1, a package of ab initio programs*, 2010, see http://www.molpro.net
[32] E. A. Pazyuk, A. V. Stolyarov, and V.I. Pupyshev, Chem. Phys. Lett. **228**, 219 (1994).
[33] D. Pavolini, T. Gustavsson, F. Spiegelmann, and J.-P. Daudey, J. Phys. B **22**, 1721 (1989).
[34] A. Zaitsevskii, E. A. Pazyuk, A. V. Stolyarov, O. Docenko, I. Klincare, O. Nikolyaeva, M. Auzinsh, M. Tamanis, and R. Ferber, Phys. Rev. A **71**, 012510 (2005).
[35] See EPAPS Document No. ... for data files associated with this paper. This document can be reached via a direct link in the online article's HTML reference section or via the EPAPS homepage (http://www.aip.org/pubservs/epaps.html).